

The Connection Between Barstrength and Circumnuclear Dust Structure¹

Molly S. Peeples, Paul Martini

*Department of Astronomy, Ohio State University, 140 W. 18th Ave., Columbus, OH 43210,
 molly@astronomy.ohio-state.edu, martini@astronomy.ohio-state.edu*

ABSTRACT

We present a comparison of barstrength Q_b and circumnuclear dust morphology for 75 galaxies in order to investigate how bars affect the centers of galaxies. We trace the circumnuclear dust morphology and amount of dust structure with structure maps generated from visible-wavelength HST data, finding that tightly wound nuclear dust spirals are primarily found in weakly barred galaxies. While strongly barred galaxies sometimes exhibit grand design structure within the central 10% of D_{25} , this structure rarely extends to within ~ 10 pc of the galaxy nucleus. In some galaxies, these spiral arms terminate at a circumnuclear starburst ring. Galaxies with circumnuclear rings are generally more strongly barred than galaxies lacking rings. Within these rings, the dust structure is fairly smooth and usually in the form of a loosely wound spiral. These data demonstrate that multiple nuclear morphologies are possible in the most strongly barred galaxies: chaotic central dust structure inconsistent with a coherent nuclear spiral, a grand design spiral that loses coherence before reaching the nucleus, or a grand design spiral that ends in a circumnuclear ring. These observations may indicate that not all strong bars are equally efficient at fueling material to the centers of their host galaxies. Finally, we investigate the longstanding hypothesis that SB(s) galaxies have weak bars and SB(r) galaxies have strong bars, finding the opposite to be the case: namely, SB(r) galaxies are less strongly barred and have less dust structure than SB(s) galaxies. In general, more strongly barred galaxies tend to have higher nuclear dust contrast.

Subject headings: dust – galaxies: ISM – galaxies: nuclei – galaxies: spiral – galaxies: structure – ISM: structure

1. Introduction

Most spiral galaxies have large-scale bars, and any complete picture of galaxies must include the impact of bars on their evolution. Bars are important because they are an obvious mechanism for funneling gas and dust to the centers of galaxies: gas clouds orbiting in the disk lose angular

¹Based on observations with the NASA/ESA *Hubble Space Telescope* obtained at the the Space Telescope Science Institute, which is operated by the Association of Universities for Research in Astronomy, Incorporated, under NASA contract NAS5-26555.

momentum as they encounter the bar, thereby sinking towards the galaxy’s center (Binney & Tremaine 1987; Athanassoula 1992; Piner et al. 1995; Regan et al. 1997; Maciejewski et al. 2002). Bars are therefore expected to play a major role in circumnuclear star formation, bulge growth, and the fueling of the central, supermassive black hole.

Bar-driven radial gas inflow should drive large quantities of gas and dust into the central regions of galaxies, thereby increasing the central gas concentration of barred galaxies relative to unbarred galaxies. Observations by Sakamoto et al. (1999) and Sheth et al. (2005) support this view, finding higher concentrations of molecular gas in the central kiloparsec of barred galaxies than in unbarred galaxies. As higher gas density is empirically correlated with higher star formation rates (e.g., Kennicutt 1998), there should be a correlation between bar-driven inflow and central star formation. Observational evidence for enhanced nuclear or circumnuclear star formation in barred galaxies provides broad support for this picture (Ho et al. 1997; Maoz et al. 2001; Knapen et al. 2006).

It has long been speculated that this same radial gas inflow could provide active galactic nuclei (AGN) with fuel (Simkin et al. 1980; Schwarz 1981). There is so far no evidence, though, that bars (large-scale or nuclear) are the primary fuel source for AGN: not all active galaxies are barred, not all barred galaxies are active, and, in fact, well-matched samples of active and inactive galaxies have the same bar fraction (Ho et al. 1997; Mulchaey & Regan 1997; Laine et al. 2002). Ho et al. speculate that this is because radially-transported gas is prevented from reaching the nucleus.

If bars are indeed fueling galaxies’ circumnuclear regions, then this should be reflected in the morphology of the cold circumnuclear interstellar medium (ISM). Martini et al. (2003a) establish a nuclear dust morphology classification system with four spiral classes (grand design, tightly wound, loosely wound, and chaotic spiral) and two non-spiral classes (chaotic and no structure) to quantify differences between various galaxy types. Martini et al. (2003b) find no differences in the nuclear dust structure of active and inactive galaxies. This study does find evidence that nuclear grand design spirals are primarily found in barred galaxies and that these grand design spirals connect to large scale dust lanes in barred galaxies. Likewise, Martini et al. primarily find tightly wound nuclear spirals in unbarred galaxies.

All of these studies of the role of bars in fueling central star formation or black holes simply compare “barred” versus “unbarred” galaxies. This discretization glosses over, and over simplifies, the long-known continuum of barstrengths (de Vaucouleurs 1959). One early way of quantifying the strength of a bar is the deprojected bar ellipticity ϵ_b (Martin 1995). The disadvantage of using the bar ellipticity is that defining the bar—i.e., its exact dimensions—is a somewhat subjective process (Buta & Block 2001). Abraham & Merrifield (2000) introduce the parameter f_{bar} , which is a function of the bar axis ratio, and therefore susceptible to the same systematics as ϵ_b . Buta & Block, by expanding on the method of Combes & Sanders (1981), circumvent this problem by using a force ratio, which they call Q_b . Assuming that the light traces the underlying mass distribution, they use near-infrared images to calculate a map of a galaxy’s potential. From these potential maps, and with some assumptions about the characteristic scale-height, they then calculate the

tangential force F_T and mean (axisymmetric) radial force $\langle F_R \rangle$. They define the ratio map Q_T as

$$Q_T(i, j) = \frac{F_T(i, j)}{\langle F_R(i, j) \rangle}. \quad (1)$$

This ratio map has the property that in each of four quadrants Q_T reaches a local extremum. Letting $Q_T^{\max, k}$ be the absolute value of such an extremum in the k th quadrant, the barstrength Q_b is defined as

$$Q_b = \frac{1}{4} \sum_{k=1}^4 Q_T^{\max, k}. \quad (2)$$

The cited uncertainties on Q_b are a measure of how much Q_T^{\max} varies by quadrant. From a comparison with the three barstrength classes defined by de Vaucouleurs (unbarred SA, weakly barred SAB, and strongly barred SB), Buta & Block find a reasonable correlation between the RC3 bar classification and Q_b , although with substantial scatter. In particular, SA galaxies have $Q_b \lesssim 0.1$, SAB galaxies have $0.05 \lesssim Q_b \lesssim 0.2$, and SB galaxies have $Q_b \gtrsim 0.15$. The most strongly barred galaxies have $Q_b \approx 0.6$ (Buta & Block 2001). While we adopt Q_b as the best available measure of barstrength, we note that Athanassoula (1992) shows that both the quadrupole moment (strength) and the pattern speed play an important role in how effectively the bar drives mass towards the center of the galaxy. Pattern speed, however, is much more difficult to measure than parameters that can be calculated from photometric data.

Martini (2004) used Q_b and the nuclear classifications of Martini et al. (2003a) to compare the barstrengths and nuclear dust morphologies of 48 galaxies with archival Hubble Space Telescope (HST) data. He found that grand design nuclear spirals are primarily found in strongly barred galaxies, while axisymmetric tightly wound nuclear spirals are exclusively found in galaxies with $Q_b < 0.1$. With a larger sample and reconsideration of the circumnuclear dust morphology classification at the smallest scales, we examine how nuclear dust structure varies with barstrength. We identify 75 galaxies, described in §2, with a measured barstrength Q_b from the literature. To analyze the dust morphology, we create “structure maps” from archival HST data using the technique of Pogge & Martini (2002) as discussed in §3.1. We then classify the galaxies according to a refined version of the classification scheme proposed in Martini et al. (2003a), as described in §3.2. The main difference between the classification scheme used here and that of Martini et al. (2003a) is a stronger focus on the central-most regions of the galaxy. We discuss our results in §4.

2. Data

We began our study with a data set of 127 galaxies with both a measured barstrength (primarily from the Ohio State University Bright Galaxy Survey (OSUBGS) by Laurikainen et al. 2004) and archival HST data. The HST images were obtained with WFPC2, with the exception of three images from the Advanced Camera for Surveys (ACS), and most employed either the F606W or F814W filters. The galaxies studied by the OSUBGS were selected to be a representative sample

of the nearby universe; specifically, based on the RC3 T-type distribution ($0 \leq T \leq 9$, or S0/a to Sm) to ensure there is no morphological selection bias (Eskridge et al. 2002).

Table 1. Data

Galaxy	Nuclear Class	Q_b	σ_{sm} ($\times 10^{-2}$)	Detector	Filter	HST Prop. ID	T	D (Mpc)	r_c (pc)	Notes
(1)	(2)	(3)	(4)	(5)	(6)	(7)	(8)	(9)	(10)	(11)
NGC289	LW	0.212 \pm 0.003	1.280 \pm 0.030	PC1	F606W	6359	4	19.4	221 ^d	SB(rs)
NGC488	LW	0.032 \pm 0.003	0.951 \pm 0.015	PC1	F606W	6359	3	29.3	447	
NGC613	CS	0.401 \pm 0.045	4.469 \pm 0.017	WF3	F606W	9042	4	17.5	280	SB(rs)
NGC864	CS	0.360 \pm 0.037	3.726 \pm 0.064	PC1	F606W	8597	5	20	177	LGD
NGC972	C	0.220 \pm 0.060 ^a	3.948 \pm 0.060	PC1	F606W	6359	2	21.4	206	
NGC1068	C	0.165 \pm 0.010	4.204 \pm 0.072	PC1	F606W	8597	3	14.4	134 ^d	
NGC1073	C	0.607 \pm 0.013	1.839 \pm 0.013	WF3	F606W	9042	5	15.2	217	SB(rs)
NGC1097	LW	0.279 \pm 0.048	2.416 \pm 0.025	HRC	F814W	9788	3	14.5	394	SB(s), LGD
NGC1241	LW	0.251 \pm 0.028	3.383 \pm 0.037	PC1	F606W	5479	3	46.6	382	SB(rs), LGD
NGC1300	LW	0.537 \pm 0.011	2.362 \pm 0.025	PC1	F606W	8597	4	18.8	311 ^d	SB(rs), LGD
NGC1317	CS	0.085 \pm 0.007	1.910 \pm 0.023	PC1	F606W	5446	1	16.9	135	LGD
NGC1326	CS	0.160 \pm 0.020 ^b	2.506 \pm 0.019	PC1	F555W	6496	-1	16.9	191	LGD
NGC1350	C	0.243 \pm 0.039	0.863 \pm 0.008	PC1	F606W	5446	1.8	16.9	258	SB(r)
NGC1365	CS	0.400 \pm 0.110 ^a	3.892 \pm 0.008	PC1	F606W	8597	3	16.9	552	SB(s), LGD
NGC1385	C	0.319 \pm 0.030	2.298 \pm 0.024	PC1	F606W	6359	6	17.5	172	SB(s)
NGC1398	N	0.202 \pm 0.011	0.552 \pm 0.001	PC1	F606W	8597	2	16.1	332	SB(r)
NGC1433	GD	0.370 \pm 0.060 ^a	1.772 \pm 0.028	WF3	F814W	9042	2	11.6	218	SB(r)
NGC1530	TW	0.610 \pm 0.160 ^a	3.965 \pm 0.005	PC1	F606W	8597	3	36.6	487	SB(rs), LGD
NGC1637	C	0.202 \pm 0.014	2.054 \pm 0.061	WF4	F555W	9155	5	8.9	91 ^d	LGD
NGC1808	LW	0.274 \pm 0.001	5.326 \pm 0.046	PC1	F675W	6872	1	10.8	203	
NGC2196	C	0.070 \pm 0.005	0.858 \pm 0.017	PC1	F606W	6359	1	28.8	236	
NGC2442	CS	0.669 \pm 0.428	2.559 \pm 0.031	WF3	F606W	9042	3.7	17.1	273	
NGC2655	CS	0.128 \pm 0.004	1.822 \pm 0.003	PC1	F547M	5419	0	24.4	348	
NGC2775	N	0.050 \pm 0.010	0.579 \pm 0.009	PC1	F606W	6359	2	17	211	
NGC2964	C	0.310 \pm 0.003	6.463 \pm 0.162	PC1	F606W	6359	4	21.9	149 ^d	LGD
NGC2985	TW	0.056 \pm 0.001	1.608 \pm 0.033	WF2	F606W	5479	2	22.4	298	
NGC2997	TW	0.060 \pm 0.020 ^b	3.498 \pm 0.067	HRC	F555W	9989	5	13.8	358	
NGC3054	C	0.170 \pm 0.020 ^b	1.697 \pm 0.013	PC1	F606W	6359	3	26.5	207	
NGC3077	C	0.119 \pm 0.016	6.253 \pm 0.093	WF3	F814W	9144	90	2.1	33	
NGC3081	GD	0.170 \pm 0.020 ^b	2.501 \pm 0.023	PC1	F606W	5479	0	32.5	198	LGD
NGC3169	C	0.090 \pm 0.005	3.254 \pm 0.066	PC1	F547M	5149	1	19.7	250	
NGC3227	C	0.158 \pm 0.021	4.615 \pm 0.109	PC1	F606W	5479	1	20.6	181 ^d	
NGC3310	C	0.060 \pm 0.010 ^c	1.575 \pm 0.007	PC1	F814W	6639	4	18.7	168	
NGC3338	TW	0.083 \pm 0.005	1.318 \pm 0.011	WF3	F606W	9042	5	22.8	391	
NGC3359	C	0.460 \pm 0.050 ^c	1.914 \pm 0.002	WF3	F606W	9042	5	19.2	405	SB(rs)
NGC3486	GD	0.108 \pm 0.002	0.968 \pm 0.006	PC1	F606W	8597	5	12.3	165 ^d	
NGC3504	LW	0.288 \pm 0.030	3.862 \pm 0.125	PC1	F606W	5479	2	26.5	207	
NGC3898	C	0.047 \pm 0.000	0.877 \pm 0.009	PC1	F606W	6359	2	21.9	278	
NGC4027	C	0.623 \pm 0.008	2.143 \pm 0.021	PC1	F814W	8599	8	25.6	175 ^d	SB(s)
NGC4030	TW	0.060 \pm 0.013	2.193 \pm 0.026	PC1	F606W	6359	4	25.9	314	
NGC4051	CS	0.280 \pm 0.008	2.873 \pm 0.082	PC1	F606W	5479	4	17	260	
NGC4138	C	0.046 \pm 0.007	2.829 \pm 0.008	PC1	F547M	6837	-1	17	127	
NGC4254	LW	0.122 \pm 0.029	2.640 \pm 0.029	PC1	F606W	8597	5	16.8	262	
NGC4303	LW	0.259 \pm 0.044	3.928 \pm 0.062	HRC	F555W	9776	4	15.2	218 ^d	LGD
NGC4314	LW	0.442 \pm 0.024	1.390 \pm 0.029	PC1	F606W	8597	1	9.7	118	SB(rs), LGD

For each galaxy, we define a critical “central” radius r_c by

$$r_c = \min\{r_{\text{eff}}(\text{bulge}), 0.01 \cdot D_{25}\}, \quad (3)$$

where $r_{\text{eff}}(\text{bulge})$ is the bulge radius reported in Laurikainen et al. (2004) and D_{25} is the RC3 value of the 25th magnitude B-band isophotal diameter (de Vaucouleurs et al. 1991). If Laurikainen et al. give no bulge radius, or if the galaxy is completely bulgeless, then $r_c = 0.01D_{25}$. A circle of radius r_c , which corresponds to 30–550 pc projected, is included on the structure maps used for classification (see §3.2). Most (about 80%) of the galaxies in the final sample have $r_c = 0.01D_{25}$.

Objects with high inclination (axis ratio $R_{25} \leq 0.30$) or low signal-to-noise ratio ($\lesssim 10$) are excluded from the sample. We also discard low-resolution objects, given by $r_c \leq 20$ resolution elements, as well as ones with unfavorable location on the chip or highly saturated centers. In general, the objects failing the resolution or signal-to-noise ratio cuts have no clearly discernible coherent spiral arm structure. All objects are closer than 50 Mpc. Our final sample, summarized in Table 1, consists of the 75 galaxies which pass our resolution and signal-to-noise ratio cuts; the T-type distribution of the Eskridge et al. sample is roughly maintained.

3. Analysis

We employ two methods of examining the nuclear dust content in galaxies. The first is to look at what structures the dust forms, i.e., a morphological classification, and the second is to simply study the amount of dust structure in the central regions. We describe in §3.1 how we use the structure map technique of Pogge & Martini (2002) to enhance dust structures on the scale of 1–15 pc. We then use these structure maps to classify the circumnuclear dust morphology into six classes (four types of spirals, plus chaotic and no structure), as described in §3.2. In §3.3 we describe how we estimate the relative amounts of central dust structure in different galaxies. Finally, in §3.4, we discuss how we statistically compare pairs of distributions of galaxies.

3.1. Structure Maps

As it is difficult to obtain a large sample of high quality, high resolution multi-band (e.g., both V and H) data, we used the “structure map” technique developed by Pogge & Martini (2002) to enhance the observable dust structure in each galaxy. Structure maps can be thought of as “single-band color maps;” while requiring data in only one band, they provide a sharp contrast between dust and star-forming regions. Martini & Pogge (1999) note that the regions of highest contrast in $V - H$ color maps are primarily due to absorption by dust structures in the V image alone, while the smoother H -band images trace the underlying stellar population. Therefore, the H -band images serve mostly to subtract larger-scale surface brightness variations from the V -band images in the $V - H$ color maps. By making structure maps from images taken at visible wavelengths, it is possible to enhance the structure due to dust and emission regions. Furthermore, as visible-

Table 1—Continued

Galaxy	Nuclear Class	Q_b	σ_{sm} ($\times 10^{-2}$)	Detector	Filter	HST Prop. ID	T	D (Mpc)	r_c (pc)	Notes
(1)	(2)	(3)	(4)	(5)	(6)	(7)	(8)	(9)	(10)	(11)
NGC4321	LW	0.183 ± 0.027	2.123 ± 0.045	PC1	F702W	5195	4	16.8	362	LGD
NGC4414	LW	0.149 ± 0.003	1.857 ± 0.032	PC1	F606W	8597	5	9.7	118	
NGC4450	C	0.131 ± 0.011	0.634 ± 0.005	PC1	F814W	5375	2	16.8	256	
NGC4501	LW	0.072 ± 0.026	1.834 ± 0.023	PC1	F606W	6359	3	16.8	276 ^d	
NGC4504	C	0.136 ± 0.019	1.723 ± 0.016	WF3	F814W	9042	6	19.5	248	
NGC4579	CS	0.197 ± 0.020	1.713 ± 0.032	PC1	F547M	6436	3	16.8	288	
NGC4593	LW	0.309 ± 0.020	1.963 ± 0.069	PC1	F606W	5479	3	39.5	447	SB(rs), LGD
NGC4651	GD	0.120 ± 0.046	1.329 ± 0.022	PC1	F555W	5375	5	16.8	195	
NGC4698	N	0.084 ± 0.040	0.700 ± 0.006	PC1	F606W	6359	2	16.8	195	
NGC4736	LW	0.048 ± 0.004	1.684 ± 0.003	PC1	F555W	5741	2	4.3	140	
NGC4939	C	0.128 ± 0.052	2.297 ± 0.008	PC1	F606W	5479	4	17.3	113	
NGC4941	CS	0.056 ± 0.008	1.582 ± 0.017	PC1	F606W	8597	2	44.3	531 ^d	LGD
NGC5054	CS	0.090 ± 0.023	1.790 ± 0.032	PC1	F606W	8597	4	9.7	102	
NGC5121	GD	0.024 ± 0.007	3.457 ± 0.003	PC1	F606W	6359	1	27.3	340 ^d	
NGC5194	LW	0.160 ± 0.000 ^c	1.198 ± 0.006	PC1	F547M	5123	4	22.1	125	
NGC5236	C	0.190 ± 0.040 ^b	1.942 ± 0.027	PC1	F814W	8234	5	7.7	251	
NGC5248	TW	0.269 ± 0.064	1.717 ± 0.027	PC1	F814W	6738	4	2.7	92 ^d	
NGC5427	LW	0.231 ± 0.074	2.327 ± 0.010	PC1	F606W	5479	5	22.7	376 ^d	LGD
NGC5643	GD	0.415 ± 0.013	1.150 ± 0.007	PC1	F606W	8597	5	38.1	312	LGD
NGC6217	C	0.360 ± 0.010 ^c	6.472 ± 0.171	PC1	F606W	5479	4	23.9	210	SB(rs)
NGC6221	C	0.436 ± 0.112	5.053 ± 0.010	PC1	F606W	5479	5	19.4	200	SB(s)
NGC6300	CS	0.187 ± 0.002	2.505 ± 0.074	PC1	F606W	5479	3	14.3	186	SB(rs), LGD
NGC6384	C	0.136 ± 0.020	0.910 ± 0.009	PC1	F606W	6359	4	26.6	477	
NGC6814	GD	0.070 ± 0.010 ^a	1.585 ± 0.049	PC1	F606W	5479	4	22.8	205	
NGC6951	LW	0.280 ± 0.040 ^a	2.036 ± 0.041	PC1	F606W	8597	4	24.1	273	LGD
NGC7098	C	0.200 ± 0.020 ^b	0.856 ± 0.003	PC1	F555W	6633	1	29.1	345	
NGC7213	TW	0.023 ± 0.002	1.124 ± 0.020	PC1	F606W	5479	1	22	198	
NGC7479	C	0.696 ± 0.060	2.022 ± 0.046	PC1	F814W	6266	5	32.4	384	SB(s)
NGC7552	LW	0.395 ± 0.044	5.391 ± 0.267	PC1	F606W	5479	2	19.5	192	SB(s)
NGC7727	LW	0.096 ± 0.024	1.222 ± 0.031	PC1	F555W	7468	1	23.3	317	

Note. — literature data and measurements for the 75 galaxies in our sample. The classification codes in column 2 are: GD: grand design nuclear spiral; TW: tightly wound spiral; LW: loosely wound spiral; CS: chaotic spiral; C: chaotic circumnuclear dust; N: no circumnuclear dust structure. These codes are defined in §3.2. Q_b (col. [3]) is from Laurikainen et al. (2004) unless otherwise noted. See §3.3 for a discussion of the structure map rms σ_{sm} (col. [4]). In column 5, “HRC” is the High Resolution Channel for ACS; the other detectors refer to different chips on WFPC2. The Hubble T-types (col. [8]) and SB classifications (col. [11]) are from the RC3. The distances (col. [9]) are from Tully & Fisher (1988) and assume $H_0 = 75 \text{ km s}^{-1} \text{ Mpc}^{-1}$. The solid white circles in Fig. 1 have radius r_c (col. [10]) as defined in eqn. (3). LGD (col. [11]) refers to “large grand design” structure; see §4.1 for details.

^aBlock et al. (2004)

^bButa & Block (2001)

^cLaurikainen & Salo (2002)

^d $r_c = r_{\text{eff}}(\text{bulge})$

wavelength images from HST have higher resolution than those in the near infrared (both being diffraction limited), a structure map can make the most of high quality data.

The structure map is mathematically defined as

$$S = \left[\frac{I}{I \otimes P} \right] \otimes P^t, \quad (4)$$

where S is the structure map, I is the image, P is the point spread function (PSF), P^t is the transform of the PSF, and \otimes is the convolution operator. Structure maps bring out variations on the smallest resolvable scale of the image, i.e., that of the PSF. For our objects, this corresponds to a projected scale of 1–15pc. The PSFs are modelled using the TinyTim software (Krist & Hook 1999).

Formally, structure maps are similar to the second-order iteration of the Richardson-Lucy (R-L) image correction (Richardson 1972; Lucy 1974). At this step in the image restoration, the first-order, smooth structure of the image has been removed, but the structures on the scale of the size of the PSF remain. Structure maps for the 75 galaxies in our sample are given in Figure 1; in all of the structure maps presented in this paper, the dusty regions appear dark while enhanced stellar light and emission-line regions are bright (e.g., the F606W filter admits several bright emission lines.)

3.2. Nuclear Dust Classification

We classify the galaxies according to a refined version of the nuclear classification scheme presented in Martini et al. (2003a). The main distinction between the scheme used here and the original one is that we have a stronger emphasis on the central-most regions of the galaxy; other differences between the scheme used here and the one in Martini et al. (2003a) are discussed below. The structure maps used for classification are scaled to have a width and height equal to 5% of D_{25} . The classification scheme uses six categories:

Grand Design (GD): Two spiral arms symmetric about a 180° rotation, at least one of which extends all the way to the unresolved nucleus of the galaxy, and at least one of which is a dominant feature

Tightly Wound (TW): Coherent spiral arm structure over a large range in radius; pitch angle less than or equal to 10°

Loosely Wound (LW): Coherent spiral arm structure over a large range in radius; pitch angle greater than 10°

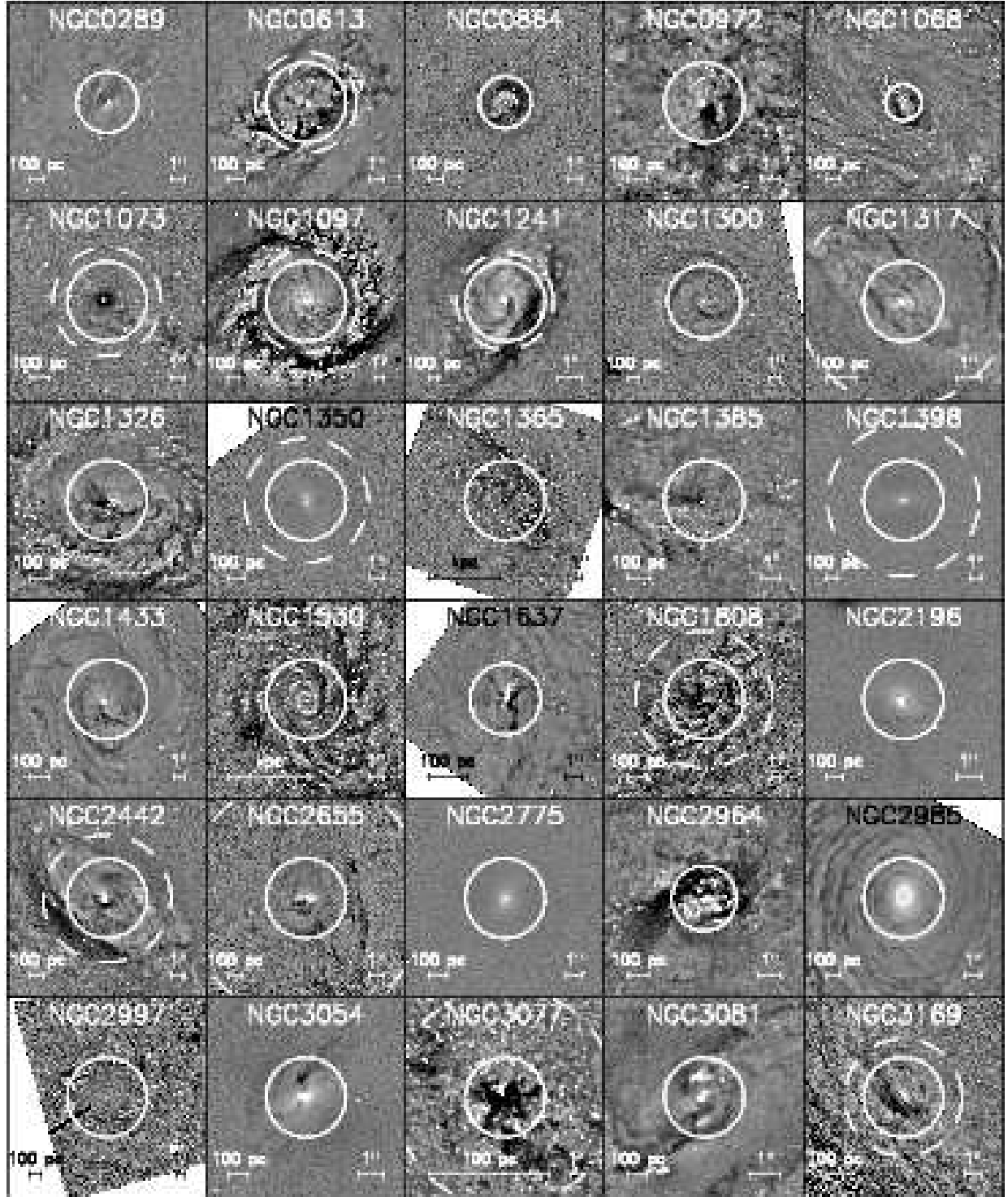


Fig. 1.— Structure maps for 75 galaxies with measured barstrengths. Each panel shows the inner 5% of D_{25} from the RC3 catalog. The solid white circles have a radius of r_c , as defined in eq. (3). In the case that $r_{\text{eff}}(\text{bulge}) > r_c$, the bulge radius is marked by a dashed white circle; these dashed circles were not included on the structure maps used for classification, but are merely given here for reference. Dark regions are due to dust, while bright regions are due to emission. Several images (e.g., NGC2997) also include the ACS coronographic finger. North is up and East is to the left.

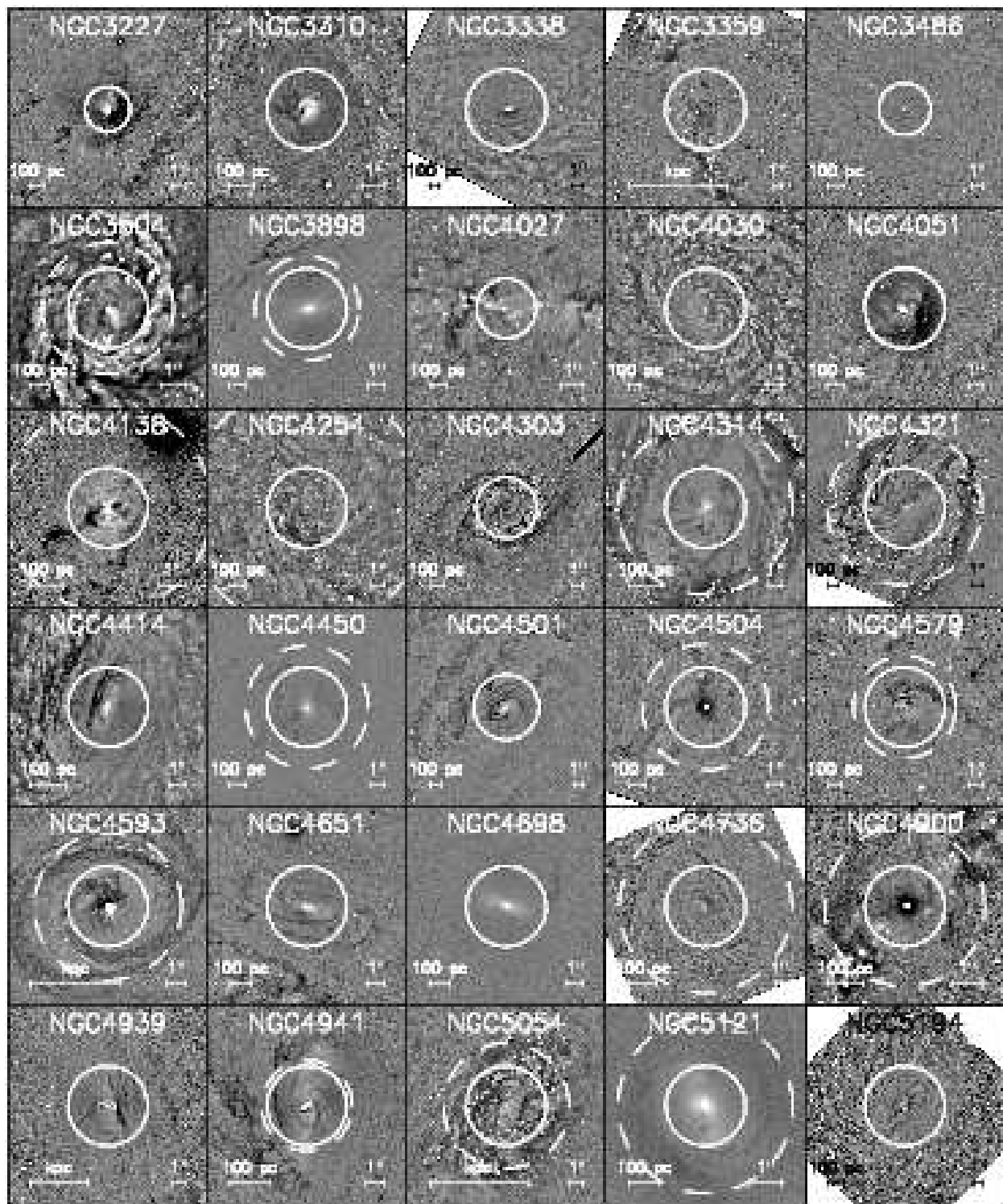


Fig. 1.— continued

Chaotic Spiral (CS): Unambiguous evidence for spiral arm structure with a unique sense of chirality, but not coherent over a large range in radius

Chaotic (C): Dust structure with no evidence of spiral structure

No Structure (N): No discernible dust structure within the central region

Examples of each classification are given in Figure 2, and the classifications for all of the galaxies in our sample are given in Table 1. There are several subtle, yet important, refinements to the original classification scheme. First, the classification is based on a region that scales with the size of the galaxy (D_{25}) rather than within the central 19.6" used by Martini et al. (2003a). Most changes in classification can be attributed to this more physically defined focus. The largest difference in an individual class is the requirement that for an object to be classified as GD, at least one of the arms must be observed to extend to the nucleus of the galaxy. For this reason, some galaxies previously classified as GD now have a different classification (e.g., NGC1365). We comment on this distinction in greater detail in §4.1.

We also quantify the distinction between tightly and loosely wound circumnuclear spirals by setting 10° as the delineation between “small” and “large” pitch angles. This division roughly corresponds to that of Sb galaxies (Kennicutt 1981). Previously, the differentiation between TW and LW was done purely by eye, and also took into account arm morphology. Specifically, for a nuclear spiral to be classified as “tightly wound,” the arms had to be traceable through at least one complete revolution, and therefore the classification was potentially subject to signal-to-noise ratio bias (for an arm to remain coherent about an entire revolution, and thus be classified as TW, a higher SNR was needed). We measure pitch angles with an interactive PGPlot program which fits logarithmic spirals to a deprojected image of the structure map. Five points of increasing radius on a single prominent spiral arm of the galaxy are chosen within an annulus given by 25–75% of the bulge radius, or of 1% of D_{25} if the galaxy is either bulgeless or there is no available effective bulge radius data.¹ The program then fits logarithmic spirals to each consecutive pair of points, averaging the resulting four pitch angles to give the pitch angle for the entire arm. As found by Kennicutt (1981) for large-scale spirals, the nuclear spirals are not well fit by logarithmic spirals—a given arm does not have constant pitch angle as a function of radius. Still, this method yields an “average” pitch angle for the arm. The observed non-constant pitch angle along a spiral arm implies that the region is experiencing differential rotation which is inconsistent with solid-body rotation (Maciejewski 2004). We also note that the pitch angle often varies between different arms in a single galaxy. Notwithstanding these caveats, we find that this method suffices for determining whether or not the pitch angle is above or below 10° , thus differentiating between TW and LW nuclear spirals.

¹This radius is distinct from r_c in that if Laurikainen et al. (2004) report a non-zero bulge radius, then it is used, rather than taking the minimum of $r_{\text{eff}}(\text{bulge})$ and $0.01D_{25}$. This is because at larger radii, there is more likely to be a coherent arm with a measurable pitch angle.

Finally, the “central region” used in classifying the N class of objects was previously defined as a “few hundred parsecs” (Martini et al. 2003a). We have clarified this so that the central region is specific to each galaxy, namely, a circle of radius r_c . This region is also used as a guide in deciding between different classifications; if a galaxy is seen to have a different morphology at small radii than at large radii, such as is seen in NGC1068, the classification at small radii is used. This decision also led to changes in the classifications of several galaxies from those reported in previous papers.

3.3. Dust Contrast

To quantify the amount of dust structure in one galaxy as compared to another, we calculated the root mean squared (rms) of the pixel-to-pixel variations of the galaxies’ structure maps within r_c . Roughly speaking, the more dust in a galaxy, the higher the dust contrast in the structure map, and therefore the higher the rms. We assign an uncertainty to the rms by calculating the standard deviation of 11 measurements of the rms within a circular aperture ranging in radius from $0.95r_c$ to $1.05r_c$ in increments on $0.01r_c$. We further define σ_{sm} to be the average of these 11 measured rms values. The variation on σ_{sm} is found to be no more than 5% for any object. The measured rms values and uncertainties for each galaxy are given in Table 1.

Because the structure map is sensitive to structures on the scale of the PSF, rather than some physical scale, there may be a strong distance-dependent bias in σ_{sm} . We therefore tested how σ_{sm} changes for a given galaxy upon changing the resolution using a test sample of nine galaxies with high enough resolutions to meet our resolution and signal-to-noise cuts (see §2) even after being convolved with a Gaussian with a standard deviation of 2.6 pixels, which corresponds to more than doubling their distance. For each object, we convolved both the image and the PSF with a Gaussian with a standard deviation of 1.0–2.6 pixels (in 0.1 pixel increments), from which a set of 17 degraded structure maps were constructed. An example of this degradation for NGC4321 is shown in Figure 3. We then calculated σ_{sm} (and uncertainty, as described above) for each of these degraded structure maps. While σ_{sm} did change for each object, the change was found to be comparable with the calculated uncertainties for any given structure map. This implies that at these scales, the dust structure is roughly scale-invariant, in agreement with the findings of Elmegreen et al. (2002) that the power spectra of dust structure becomes relatively shallow at small scales. We thus conclude that σ_{sm} does not contain a distance-dependent bias and employ it below to compare different subsamples of galaxies.

3.4. Comparing Q_b and σ_{sm} Distributions

Once the galaxies are classified, we have sets of barstrengths Q_b and structure map rms values σ_{sm} for each nuclear classification. We then want to answer the question of how likely it is that the objects of a given classification are drawn from same parent distribution as other galaxies. The

standard method for comparing two arbitrary distributions is the Kolmogorov-Smirnov (K-S) test, which calculates the maximum vertical separation D_{KS} between two cumulative distributions. The larger the K-S distance D_{KS} for two samples, the less likely the two distributions represent the same parent population. D_{KS} only takes on discrete values, namely, multiples of $1/(N_A + N_B)$, where N_A and N_B are the number of elements in the two samples A and B under comparison. To compare two samples, we first calculate the distance D_{KS} between the two distributions. Then, for 10,000 trials, we compare this D_{KS} to the distance between two samples of size N_A and N_B drawn from a uniform distribution, yielding a probability that the two samples are in fact drawn from the same distribution. These probabilities do not change significantly when errors on Q_b or σ_{sm} are taken into account. In the event that the two samples intersect, we exclude the shared galaxies from both samples in order to do the comparison.

In the few cases where both sample sizes small, we use the Wilcoxon rank-sum test instead of the K-S test. The Wilcoxon test compares two samples A and B of size N_A and N_B , with $N_A \leq N_B$, where the “true” mean values of A and B are μ_A and μ_B , respectively. Letting the sum of the ranks in sample A be w , the probability that $\mu_A > \mu_B$ is equal to the probability that the sum of the ranks of N_A randomly chosen elements (from a set of size $N_A + N_B$) is $\leq w$, while the probability that $\mu_A < \mu_B$ is equal to the probability that the sum of ranks is $\geq N_A(N_A + N_B + 1) - w$.

4. Results and Discussion

Our classifications and measurements of σ_{sm} are summarized in Table 1. There is a 2% probability that the tightly wound (TW) nuclear dust spirals have the same underlying distribution of barstrength as the rest of the sample. As shown in Figure 4, TW nuclear spirals are found primarily—although not exclusively—in weakly barred galaxies. As the TW class is defined to be those dust spirals with pitch angle $\leq 10^\circ$, this is consistent with the idea that a galaxy which is axisymmetric at large scales (i.e., has a small Q_b) will either have high differential rotation or simply that the central regions of these galaxies cannot be highly disrupted. All four late-type galaxies in our sample ($T \geq 6$) have chaotic circumnuclear dust structure, as shown in the right-hand panel of Figure 5. No such differences were found for any other nuclear class,² as shown in the left-hand panel of Figure 5 and Figure 6. As previous studies have suggested a connection between large-scale bars and grand design nuclear spirals, we begin our discussion of strongly barred galaxies below with a consideration of grand design nuclear spirals.

4.1. Circumnuclear Grand Design Spirals

Hydrodynamic simulations suggest that large-scale bars can lead to the formation of grand design nuclear spirals (Patsis & Athanassoula 2000; Englmaier & Shlosman 2000), and several

²While all three N class galaxies have a $T = 2$ (corresponding to a Hubble type of Sab), this is not significant.

observational studies support this hypothesis (Pogge & Martini 2002; Martini et al. 2003b). With our focus on the very central regions of nuclear spirals, we find that this is in fact not the case: the grand design nuclear spirals described in §3.2 are *not* preferentially found in strongly barred galaxies. We find, however, that symmetric two-arm spiral structure is common at larger scales in strongly barred galaxies. To differentiate between circumnuclear grand design spirals found at different scales, we hereafter refer to grand design structure at small radii, defined as GD in §3.2, as SGD structure (small grand design), and prominent grand design structure at larger radii (within 10% of D_{25} , as shown in Figure 7) as LGD structure (large grand design).

Figure 7 shows four examples of galaxies for which grand design structure is evident at larger scales, but is not present at smaller scales. Seven galaxies (9% of the entire sample) have SGD structure, while twenty (26%) have LGD structure. This larger-scale GD structure extends to the center of the galaxy in only two (10%) of these twenty galaxies. As can be seen in Figure 8, LGD galaxies are preferentially more strongly barred than SGD galaxies. A K-S test excluding the two shared galaxies reveals a 3% probability that SGD and LGD barstrengths are drawn from the same parent distribution. We further find a 0.4% probability that LGD galaxies have the same underlying distribution of Q_b as the other 59 galaxies in the sample; galaxies with LGD nuclear spirals are more strongly barred than other galaxies.

Visually, SGD galaxies seem to have less circumnuclear dust than their LGD counterparts. A K-S test comparing the σ_{sm} values of the two samples supports this impression, yielding a 3% probability that the two are drawn from the same parent distribution (see Figure 8). This is in agreement with the overall trend discussed below in §4.2 that more strongly barred galaxies have dustier circumnuclear regions, suggesting that the gas and dust funnelled to the center of a barred galaxy may eventually suffice to disintegrate a symmetric two-armed spiral in the central few hundred parsecs. The most likely mechanism for erasing the small-scale spiral structure is energy feedback from substantial star formation. We note that many of the galaxies with the largest σ_{sm} (e.g., NGC1808, NGC2964, NGC6217 and NGC7552) are well-known starbursts or nuclear starbursts. This indicates that there may be sufficient feedback from star formation to shape the structure of the circumnuclear ISM.

4.2. Circumnuclear Rings and Strongly Barred Galaxies

The material funnelled inward by the large-scale bar may not reach the central region at all, but instead form a circumnuclear starburst ring. If bars prompt rings of circumnuclear star formation, then star-forming rings should be more prevalent in strongly barred galaxies than in weakly barred ones. Observations do suggest that barred galaxies have a higher incidence of nuclear starburst rings than unbarred galaxies (see Kormendy & Kennicutt 2004, and references therein). We offer here more evidence that this is in fact the case.

Of the 75 galaxies studied, eight have circumnuclear starburst rings visible at radii less than

or equal to 5% of D_{25} . All eight exhibit LGD structure,³ as shown in Figure 10. One interesting transition case is NGC5427, where the LGD spiral arms appear to become the incomplete starburst ring itself. NGC4314 also exhibits this morphology, although the ring is more complete. The LGD dust lanes enter a number of other rings (e.g., NGC1097 and NGC6951), but these “breaks” may simply be due to dust attenuation of a complete ring. As seen in Figure 1, the effective bulge radius and the circumnuclear ring radius for each of these galaxies apparently coincide. Of these eight galaxies, six have loosely wound circumnuclear spirals within the ring, while the other two (NGC864 and NGC1326) have chaotic circumnuclear spirals. Only 32 of the 75 galaxies are LW or CS; according to a binomial distribution, the probability of randomly selecting 8 galaxies that are restricted to these two classes is 0.062%. The circumnuclear morphology within a circumnuclear ring is therefore distinct from the ring itself. Visually, the rings appear highly turbulent and almost flocculent, while the dust structure in their interiors is much smoother.

The galaxies with circumnuclear rings are also, as a group, more strongly barred than typical galaxies. The K-S test gives a probability of 1.5% that the ringed galaxies have the same barstrength distribution as the other 67 galaxies, and a probability of 3% that the LW ringed galaxies have the same distribution of barstrengths as the other fourteen LW galaxies. The barstrengths of the entire, LW, and ringed galaxy samples are shown in Figure 9.

There remain many pieces needed to assemble the circumnuclear starburst ring puzzle. A large-scale bar drives dust and gas towards the center of the galaxy. At the boundary of the bulge and the disk, a starforming ring develops. Within this ring, there is a fairly coherent loosely wound dust spiral. It is unclear, however, whether this nuclear dust spiral is composed of dust and gas originating from the large-scale bar and/or the ring itself, or if it is native dust that is “stirred-up” by the starburst ring. Simulations by Regan & Teuben (2004) imply that bars are only capable of driving gas down to the radius at which the ring forms—but not further—suggesting that native dust comprises the nuclear spiral.

For the entire sample of 75 galaxies, we find an increase in the structure map rms σ_{sm} with the barstrength Q_b , although with substantial scatter and evidence the relation appears to turn over at large Q_b . The observed increase in dust structure may be due to increased star formation rates, which are correlated with the gas surface density via the global Schmidt law (Schmidt 1959; Kennicutt 1998). The structure maps for the twelve most strongly barred galaxies in our sample ($Q_b \geq 0.4$) are shown in Figure 11. Of these twelve, five have LGD spirals, two of which end at a circumnuclear ring. The other seven have either chaotic or chaotic spiral nuclear dust morphology (5 C, 2 CS). As a circumnuclear ring is associated with nuclear star formation, and the chaotic structures seen in these strongly barred galaxies could potentially be related to star formation, it would be interesting to investigate the relationship between nuclear star formation rates, circumnuclear dust morphology, dust structure σ_{sm} , and barstrength.

³The LGD structure in NGC1300 and NGC0864, while visible on the structure maps, is more prominent on the $V - H$ color maps of Martini et al. (2003a). This is because in these two cases, the relevant dust lanes are larger than the PSF, and thus have low contrast on the structure map.

4.3. Large-scale Morphology: SB Galaxies

One way in which barred spiral galaxies are commonly divided into subclasses is by taking note of where the large scale spiral starts with relation to the bar (e.g., Sandage & Bedke 1994). In SB(s) galaxies, the spiral arms begin at the ends of the bar, whereas in SB(r) galaxies, the spiral arms begin on a ring connecting the ends of the bar. SB(rs) galaxies are a transition group. SB(s) structures are thought to be preferentially found in less strongly barred galaxies than their SB(r) counterparts (e.g., Sanders & Tubbs 1980; Simkin et al. 1980). Furthermore, SB(s) galaxies typically show large-scale dust lanes that are not present in SB(r) galaxies, and SB(r) galaxies are observed to have less dust in their central regions than SB(s) galaxies (Kormendy & Kennicutt 2004). This is an apparent inconsistency with the generic bar-fueling picture: SB(r) galaxies are thought to have less dust—but be more strongly barred—while more strongly barred galaxies should have a higher central dust content. As these conclusions have been based on measuring the barstrength as an axis ratio (e.g., Sanders & Tubbs 1980), rather than as a force ratio, this discrepancy might be because SB(r) galaxies are actually more weakly barred than SB(s) galaxies. We reinvestigate the relation between these bar sub-types and barstrength.

The breakdown by nuclear class, including LGD, of the 21 RC3-classified SB galaxies in our sample is given in Table 2. A small increase in Q_b is seen from SB(r) to SB(s). Visually, the SB(r) galaxies have much less dust structure than the SB(rs) and SB(s) galaxies. According to the Wilcoxon test, the SB(r) sample has a smaller Q_b than the SB(s) galaxies at a confidence level of 94%. Sanders & Tubbs (1980) suggest bar pattern speed as an alternative origin to the differences in SB(r) and SB(s) structure: a slowly rotating bar should give rise to SB(r) structure, while a rapidly rotating bar should yield SB(s) structure. As the differences in barstrength are reversed from what was expected, rotation may more important in determining the large-scale morphology. With respect to the amount of dust structure, we find with $\geq 99\%$ confidence that the SB(r) galaxies have less dust structure (smaller σ_{sm}) than the SB(s) sample; similarly, we find with 97% confidence that the SB(r) sample has less dust than the SB(rs) galaxies.

	SB	SB(r)	SB(rs)	SB(s)
$\langle Q_b \rangle$	0.397	0.272	0.398	0.450
Total	21	3	11	7
GD	1	1	0	0
TW	1	0	1	0
LW	7	0	5	2
CS	3	0	2	1
C	8	1	3	4
N	1	1	0	0
LGD	6	0	6	2

Table 2: Average barstrengths and nuclear classifications for SB galaxies. Nuclear classes are defined in §3.2, and LGD morphology is defined in §4.1. SB classification is given by the RC3 catalog.

An important caveat for this aspect of our work is that large-scale morphological classifications are known to depend on wavelength. For example, while only about one third of galaxies are classified as SB at visible wavelengths, over two thirds are classified as SB in the near infrared (Eskridge et al. 2000). This is primarily because near infrared light traces the underlying stellar mass, which is also one of the main reasons Q_b is calculated using near infrared data (Buta & Block 2001). Eskridge et al. (2002) reclassify 205 spiral galaxies according to their H -band photometry from the OSUBGS. Forty-eight of our 75 galaxies are in this sample; 58% of which (28 of the 48) are classified as SB. Eskridge et al. do not, however, subclassify the H -band images into SB(r), (rs), and (s). It would be interesting to see how the dust content and Q_b vary by class in NIR-identified SB galaxies.

5. Conclusion

We present a study of the circumnuclear dust morphology for a sample of 75 galaxies with archival HST data and measured barstrength Q_b . This Q_b is a measure of the maximal force ratio due to the presence of a bar in a galaxy, and thus is arguably superior to the rudimentary bar axis ratio (Buta & Block 2001). We use the structure map technique of Pogge & Martini (2002) to enhance the visibility of the galaxies' dust content and to classify the circumnuclear dust morphology within the central 5% of D_{25} , according to a refined version of the classification scheme proposed by Martini et al. (2003a). We also introduce the structure map rms σ_{sm} within the central regions of the galaxy as a quantitative measure of the amount of nuclear dust structure. A comparison of the morphological classifications and measured barstrengths reveals that tightly wound nuclear dust spirals (with pitch angles less than 10°) are preferentially found in galaxies with lower Q_b . No other nuclear class exhibits a significant correlation with barstrength.

Previous observations found that grand design nuclear dust spirals are hosted exclusively by strongly barred galaxies. While we do see grand design structure in many barred galaxies, this grand design structure does not extend all the way into the unresolved nucleus (~ 10 pc), although it is often present at larger scales. Earlier studies did not strictly require that the grand design structure extend into the nucleus. Taking this into account, we identify two distinct types of circumnuclear grand design spirals. Small grand design (SGD) spirals are nuclear dust spirals in which the two symmetric spiral arms are coherent from 1% of D_{25} (typically a few hundred parsecs) to the central tens of parsecs of the galaxy (where tracing the structure becomes resolution-limited). Large grand design (LGD) nuclear spirals, on the other hand, show two prominent symmetric arms within 10% of D_{25} (typically on the scale of a few kiloparsecs); these arms do not necessarily extend to the center of the galaxy. In fact, these two types of grand design structure are nearly disjoint: the nuclear spiral arms in only two of the twenty LGD galaxies in our sample extend into the unresolved center of the galaxy (i.e., also displayed SGD structure). The LGD spirals are found in systematically more strongly barred host galaxies. This strongly confirms previous indications from much smaller samples and demonstrates that the dust lanes along the leading edges of large-scale spirals do not generally extend all the way into the nuclear region, but instead lose coherence at the scale of

several hundred parsecs. While SGD spirals are not found in galaxies with a significantly different barstrength than typical galaxies, they are found in galaxies with significantly less dust structure in the central regions than LGD galaxies. The reduced dust structure may reflect a requirement for the formation of SGD morphology, or simply a requirement for its detection.

The LGD spiral arms may not maintain coherence to the nucleus because mass inflow due to the presence of a large-scale bar prompts star formation, which can disrupt a nuclear grand design spiral. In addition, forty percent of the LGD spirals do not extend into the nuclear region because there is a circumnuclear starburst ring. We find that all of the galaxies with circumnuclear starburst rings have LGD structure and are more strongly barred than other galaxies. Within the rings, three fourths of the galaxies with circumnuclear rings have coherent loosely wound spirals within the ring, while the others have less coherent chaotic spirals.

We also find that among SB galaxies, SB(s) galaxies have more dust structure and are more strongly barred than SB(r) galaxies. This is partially at odds with the prevailing view in the literature, which is that SB(r) galaxies should be more strongly barred, although there is consensus that SB(r) galaxies have less central dust (e.g. Kormendy & Kennicutt 2004). Sanders & Tubbs (1980) suggest that differences in the bar pattern speed may also explain the large-scale morphological differences between SB(s) and SB(r) galaxies; as our results indicate that SB(s) galaxies are more strongly barred, pattern speed may be the more relevant parameter.

Overall, there is agreement in the literature that more strongly barred galaxies should—and do—have more dust and gas in their centers (Kormendy & Kennicutt 2004). We find that for the most strongly barred galaxies, there are several possible morphologies the circumnuclear dust can take. This may indicate that not all bars of a given strength Q_b funnel material toward the centers of galaxies with equal efficiency, potentially due to the effects of pattern speed on bar efficiency, or simply the fact that Q_b is a one-parameter description of the bar. In the most strongly barred galaxies, there can be an LGD spiral whose arms do not extend to the galaxy nucleus but instead lose coherence. Some LGD spirals end in circumnuclear starburst rings. In the absence of these structures, however, the nuclear dust in the most strongly barred galaxies tends to be fairly chaotic, potentially hosting star formation. It would be interesting to investigate how circumnuclear dust morphology and dust structure σ_{sm} varies with nuclear star formation rates in strongly barred galaxies.

We would like to thank Andy Gould and Rick Pogge for their helpful comments. Support for this work was provided by NASA through grant AR-10677 from the Space Telescope Science Institute, which is operated by the Association of Universities for Research in Astronomy, Inc., under NASA contract NAS5-26555.

REFERENCES

Abraham, R. G. & Merrifield, M. R. 2000, AJ, 120, 2835

Athanassoula, E. 1992, MNRAS, 259, 345

Binney, J. & Tremaine, S. 1987, Galactic Dynamics (Princeton, NJ, Princeton University Press)

Block, D. L., Buta, R., Knapen, J. H., Elmegreen, D. M., Elmegreen, B. G., & Puerari, I. 2004, AJ, 128, 183

Buta, R. & Block, D. L. 2001, Bulletin of the American Astronomical Society, 33, 912

Combes, F. & Sanders, R. H. 1981, A&A, 96, 164

de Vaucouleurs, G. 1959, Handbuch der Physik, 53, 275

de Vaucouleurs, G., de Vaucouleurs, A., Corwin, Jr., H. G., Buta, R. J., Paturel, G., & Fouque, P. 1991, Third Reference Catalogue of Bright Galaxies (Volume 1-3, XII, 2069 pp. 7 figs.. Springer-Verlag Berlin Heidelberg New York)

Elmegreen, D. M., Elmegreen, B. G., & Eberwein, K. S. 2002, ApJ, 564, 234

Englmaier, P. & Shlosman, I. 2000, ApJ, 528, 677

Eskridge, P. B., Frogel, J. A., Pogge, R. W., Quillen, A. C., Berlind, A. A., Davies, R. L., DePoy, D. L., Gilbert, K. M., Houdashelt, M. L., Kuchinski, L. E., Ramírez, S. V., Sellgren, K., Stutz, A., Terndrup, D. M., & Tiede, G. P. 2002, ApJS, 143, 73

Eskridge, P. B., Frogel, J. A., Pogge, R. W., Quillen, A. C., Davies, R. L., DePoy, D. L., Houdashelt, M. L., Kuchinski, L. E., Ramírez, S. V., Sellgren, K., Terndrup, D. M., & Tiede, G. P. 2000, AJ, 119, 536

Ho, L. C., Filippenko, A. V., & Sargent, W. L. W. 1997, ApJ, 487, 591+

Kennicutt, Jr., R. C. 1981, AJ, 86, 1847

—. 1998, ApJ, 498, 541

Knapen, J. H., Mazzuca, L. M., Böker, T., Shlosman, I., Colina, L., Combes, F., & Axon, D. J. 2006, A&A, 448, 489

Kormendy, J. & Kennicutt, R. C. 2004, ARA&A, 42, 603

Krist, J. E. & Hook, R. N. 1999, The Tiny Tim User's Guide (STScI: Baltimore)

Laine, S., Shlosman, I., Knapen, J. H., & Peletier, R. F. 2002, ApJ, 567, 97

Laurikainen, E. & Salo, H. 2002, MNRAS, 337, 1118

Laurikainen, E., Salo, H., Buta, R., & Vasylyev, S. 2004, MNRAS, 355, 1251

Lucy, L. B. 1974, AJ, 79, 745

Maciejewski, W. 2004, MNRAS, 354, 883

Maciejewski, W., Teuben, P. J., Sparke, L. S., & Stone, J. M. 2002, MNRAS, 329, 502

Maoz, D., Barth, A. J., Ho, L. C., Sternberg, A., & Filippenko, A. V. 2001, AJ, 121, 3048

Martin, P. 1995, AJ, 109, 2428

Martini, P. 2004, in Penetrating Bars Through Masks of Cosmic Dust, ed. D. L. Block, I. Puerari, K. C. Freeman, R. Groess, & E. K. Block, 213–222

Martini, P. & Pogge, R. W. 1999, AJ, 118, 2646

Martini, P., Regan, M. W., Mulchaey, J. S., & Pogge, R. W. 2003a, ApJS, 146, 353

—. 2003b, ApJ, 589, 774

Mulchaey, J. S. & Regan, M. W. 1997, ApJ, 482, L135

Patsis, P. A. & Athanassoula, E. 2000, A&A, 358, 45

Piner, B. G., Stone, J. M., & Teuben, P. J. 1995, ApJ, 449, 508

Pogge, R. W. & Martini, P. 2002, ApJ, 569, 624

Regan, M. W. & Teuben, P. J. 2004, ApJ, 600, 595

Regan, M. W., Vogel, S. N., & Teuben, P. J. 1997, ApJ, 482, L143+

Richardson, W. H. 1972, Optical Society of America Journal A, 62, 55

Sakamoto, K., Okumura, S. K., Ishizuki, S., & Scoville, N. Z. 1999, ApJ, 525, 691

Sandage, A. & Bedke, J. 1994, The Carnegie atlas of galaxies (Washington, DC: Carnegie Institution of Washington with The Flintridge Foundation, —c1994)

Sanders, R. H. & Tubbs, A. D. 1980, ApJ, 235, 803

Schmidt, M. 1959, ApJ, 129, 243

Schwarz, M. P. 1981, ApJ, 247, 77

Sheth, K., Vogel, S. N., Regan, M. W., Thornley, M. D., & Teuben, P. J. 2005, ApJ, 632, 217

Simkin, S. M., Su, H. J., & Schwarz, M. P. 1980, ApJ, 237, 404

Tully, R. B. & Fisher, J. R. 1988, Catalog of Nearby Galaxies (Catalog of Nearby Galaxies, by R. Brent Tully and J. Richard Fisher, pp. 224. ISBN 0521352991. Cambridge, UK: Cambridge University Press, April 1988.)

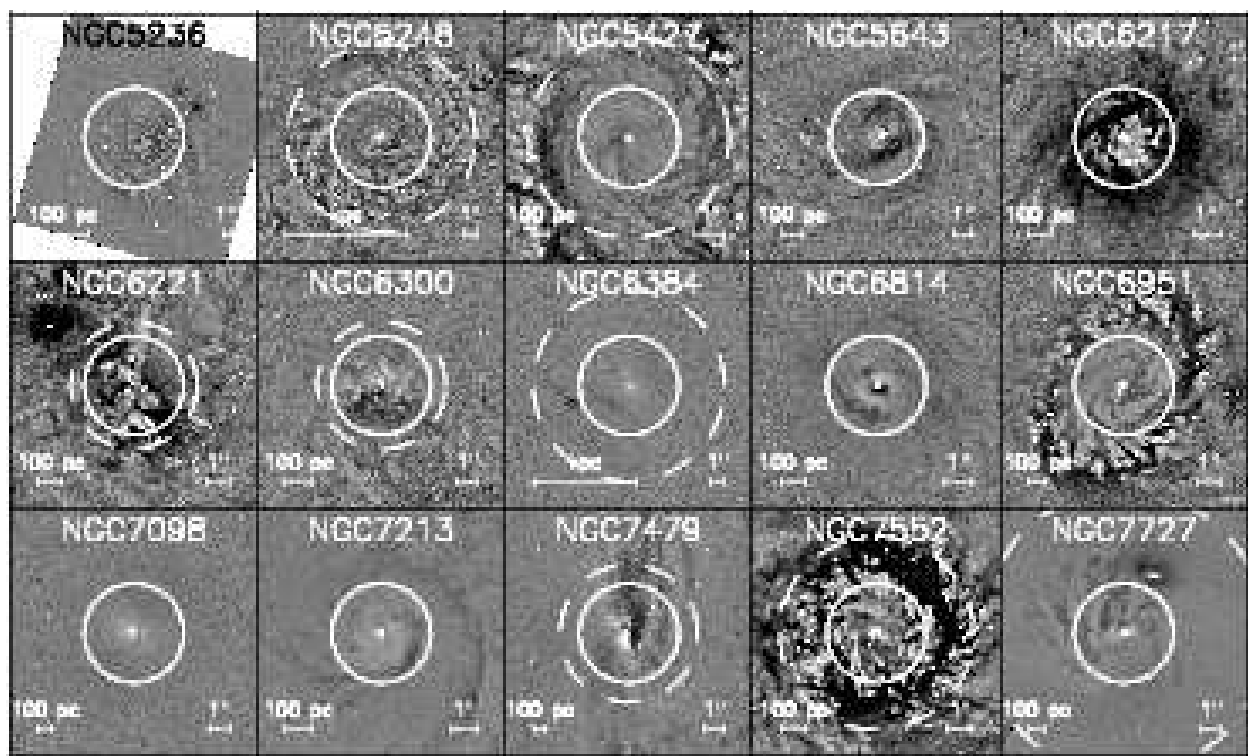


Fig. 1.— continued

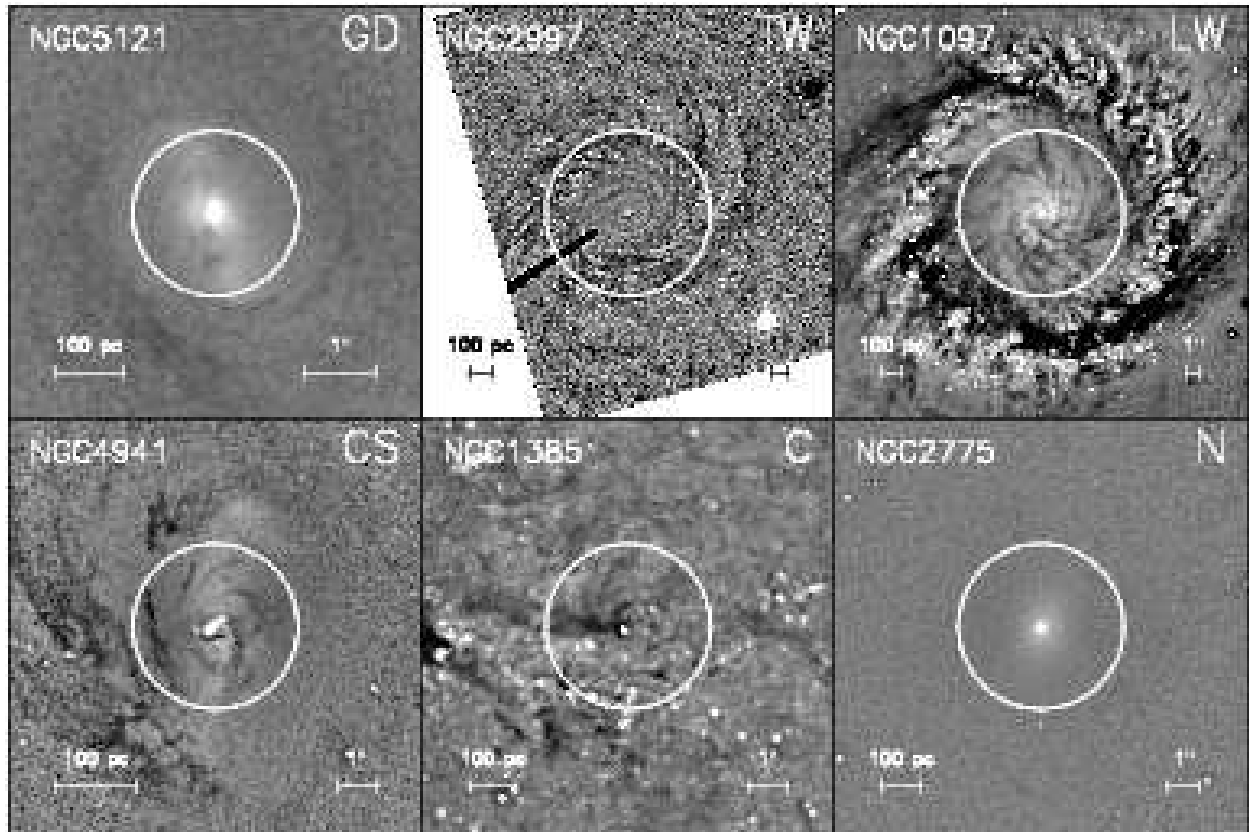


Fig. 2.— Structure maps of prototypes for the six circumnuclear morphology classes discussed in §3.2. The white circles have a radius of r_c , as defined in eq. (3). Dark regions are dust, while bright regions are emission.

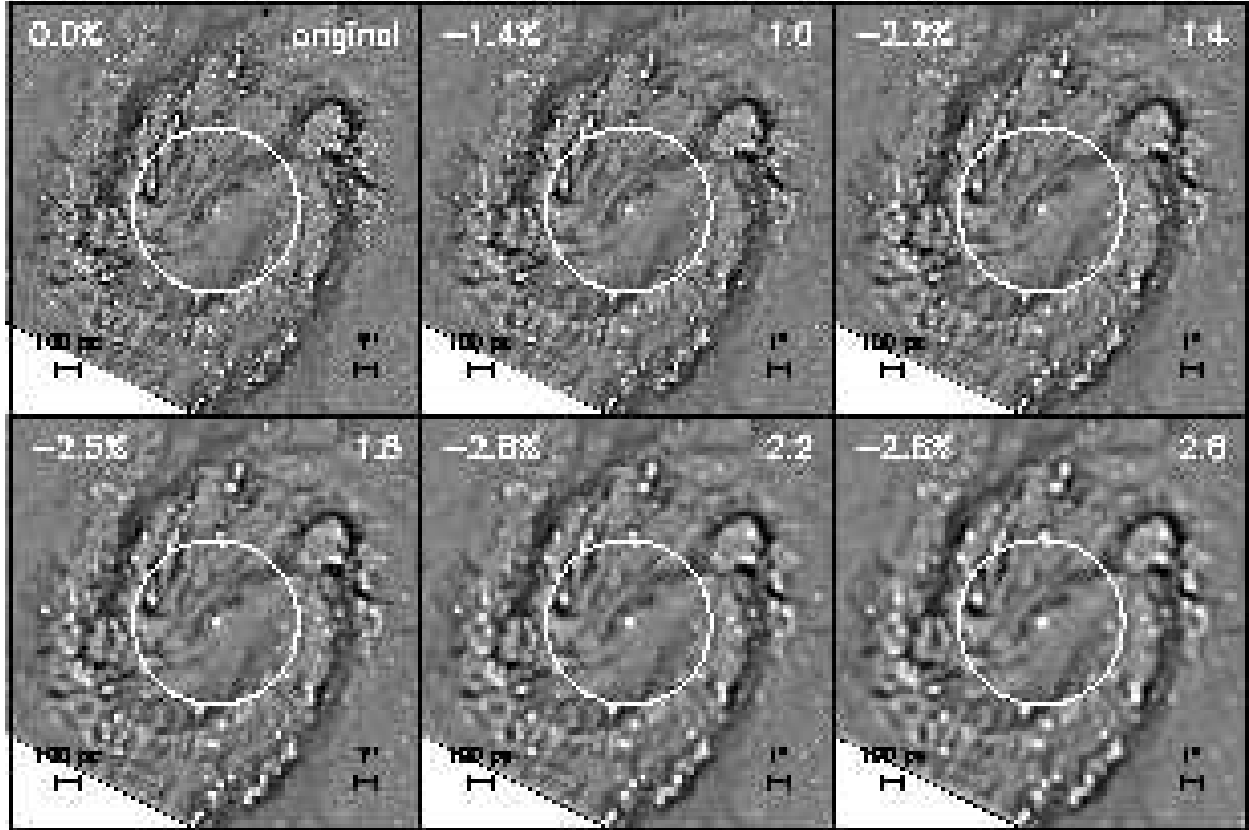


Fig. 3.— Degraded structure maps of NGC4321 for testing the dependence of structure map rms σ_{sm} on resolution. The percents in the upper left-hand corners are the percent change in σ_{sm} relative to the original structure map. The numbers in the upper right-hand corners are the standard deviations in pixels of the Gaussians with which both the image and the PSF were convolved before construction of the structure map. The white circles have a radius of r_c , as defined in eq. (3). The resolution of the original image is $0.06''$, or 4.9 pc, while the resolution of the 2.6σ Gaussian convolved image is $0.13''$, or 10.8 pc. This is equivalent to moving the galaxy from 16.8 Mpc to 37 Mpc. Relative to the measured uncertainty on the original σ_{sm} (2.1%), there is no significant change in σ_{sm} with resolution.

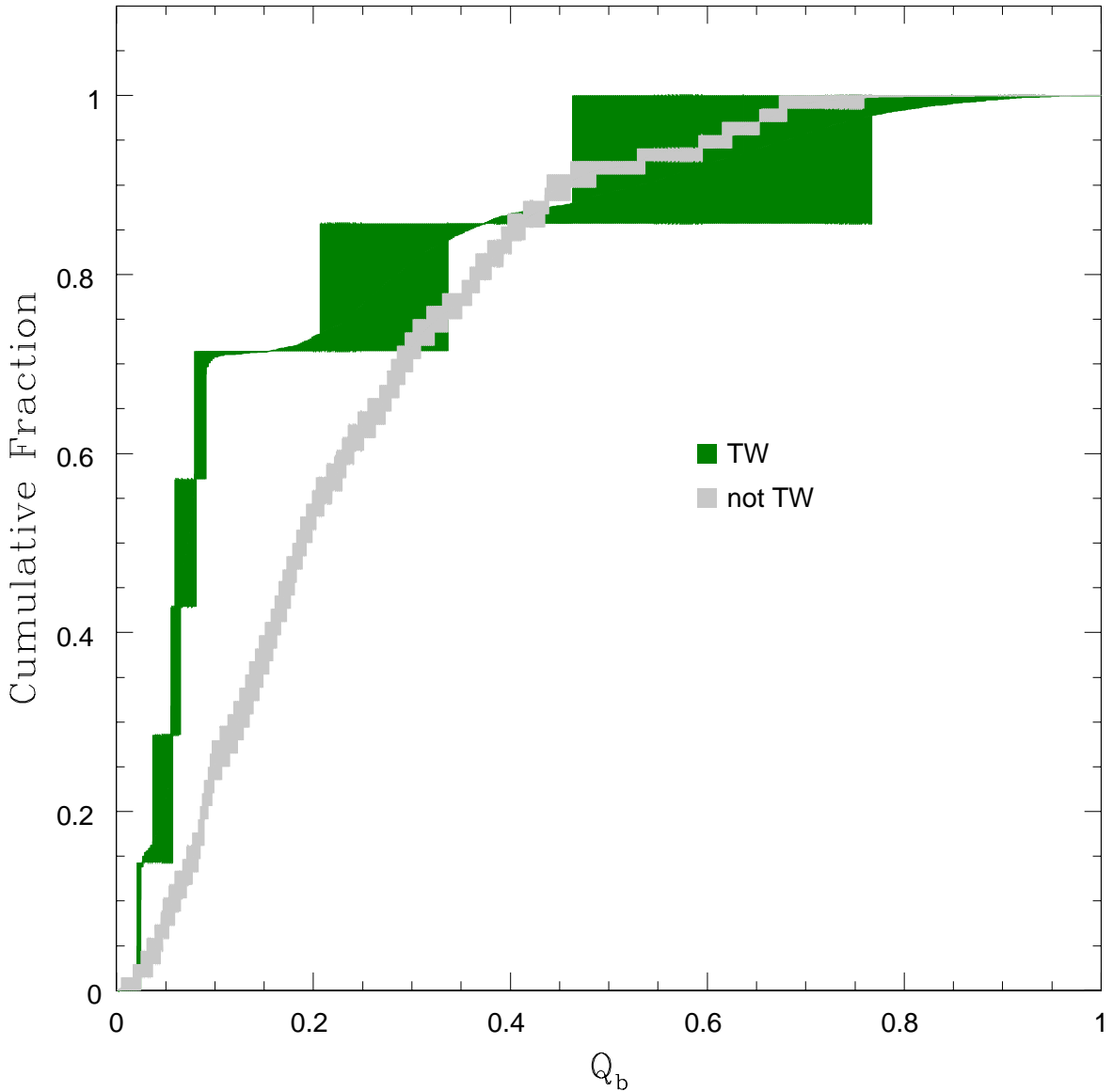


Fig. 4.— Comparison of Q_b for TW galaxies and all other galaxies. The vertical widths correspond to the central 68-percentile spread of the cumulative fraction and are due to the uncertainty in Q_b . Galaxies with TW circumnuclear dust spirals are more weakly barred than typical galaxies, with a 2% probability of being drawn from the same parent distribution.

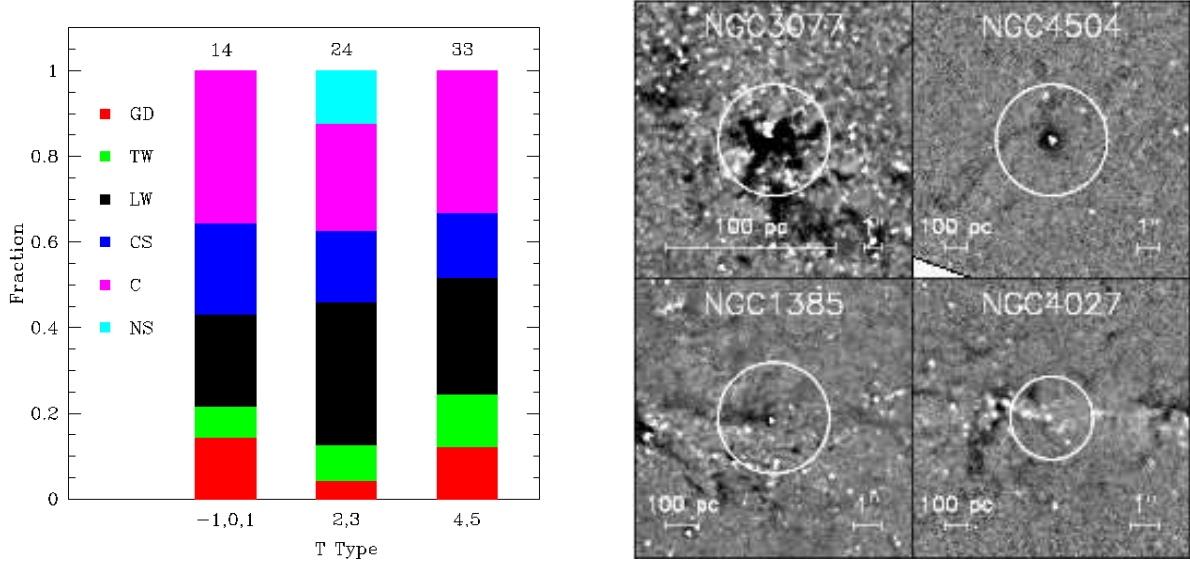


Fig. 5.— *Left*: No connection is seen between Hubble T-type for $T \leq 5$ (Sc) and nuclear classification. *Right*: Structure maps for the four galaxies in the sample with $T \geq 6$. The large scale morphologies from the RC3 catalog are: NGC3077, I0; NGC4504, Scd; NGC1385, Scd; NGC4027, Sdm. All four of these galaxies are classified as having chaotic circumnuclear dust structure.

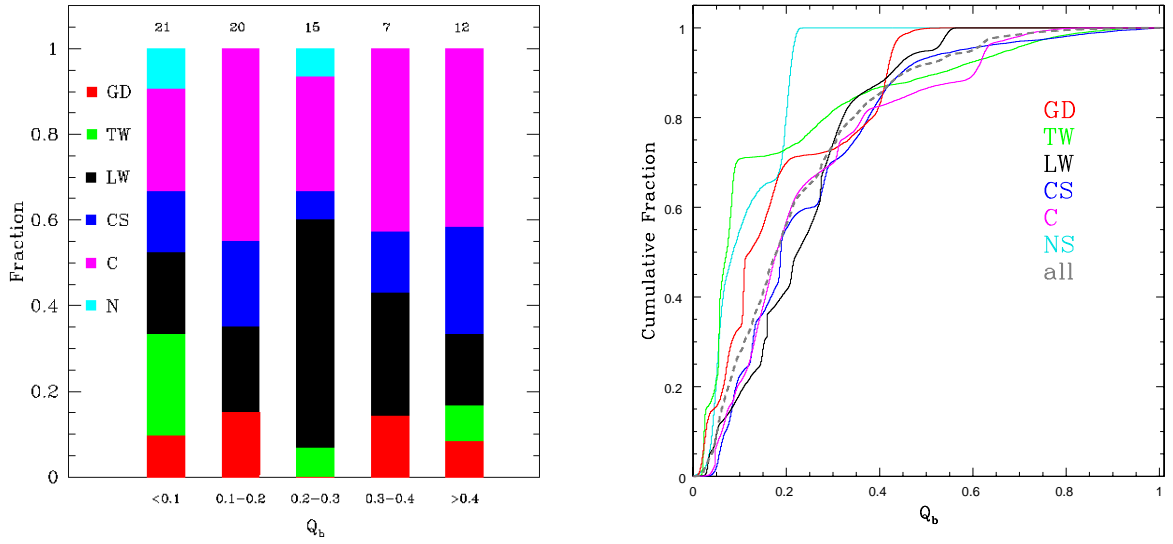


Fig. 6.— Nuclear classifications and barstrength Q_b . *Left*: Distribution of nuclear classification into different barstrength classes. *Right*: Monte Carlo average cumulative distribution of barstrength in each nuclear class and total sample.

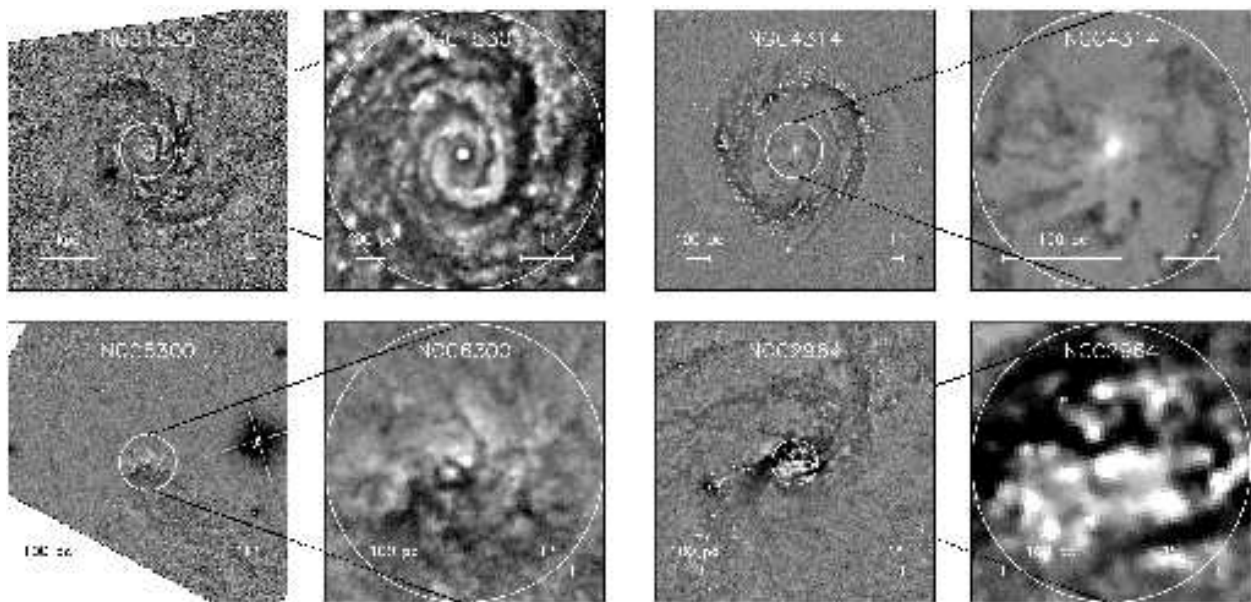


Fig. 7.— Four examples of galaxies with LGD (large grand design) but not SGD (small grand design) structure. *Left*: Width and height are given by $0.1D_{25}$. *Right*: Width and height are given by r_c . The classifications are: NGC1530, TW; NGC4314, LW; NGC6300, CS; NGC2964, C. The white circles in both panels have radius r_c . Dark regions are due to dust, while bright regions are due to emission. North is up and East is to the left.

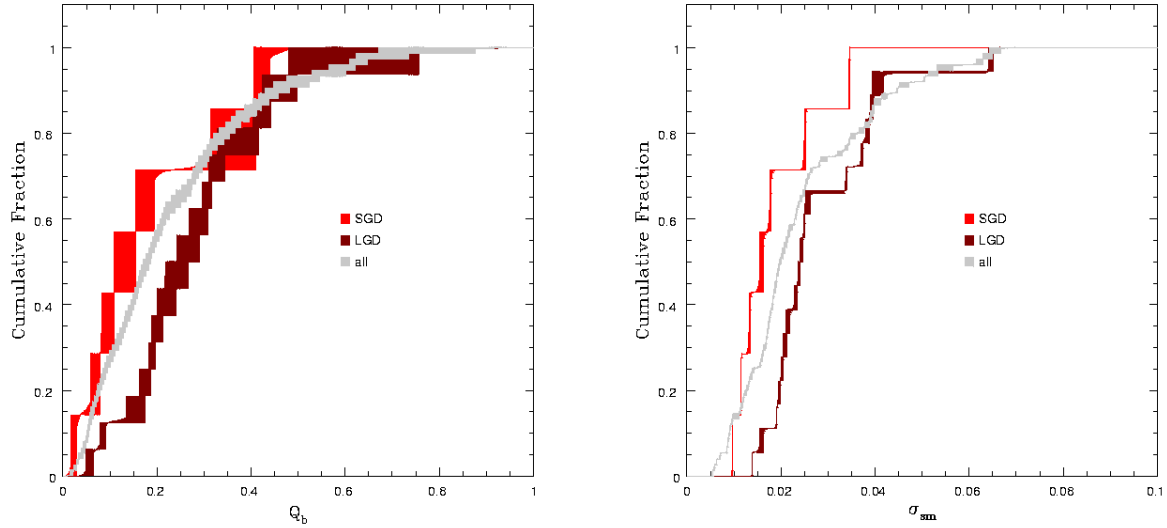


Fig. 8.— Comparisons of barstrengths Q_b and structure map rms σ_{sm} for SGD and LGD galaxies. The vertical widths correspond to the central 68-percentile spread of the cumulative fraction and are due to the uncertainty in Q_b and σ_{sm} . SGD galaxies are less strongly barred (left) and have less dust structure (right) than LGD galaxies. There is a 0.4% probability that the Q_b are drawn from the same parent population, and 3% probability that the rms values are drawn from the same parent distribution.

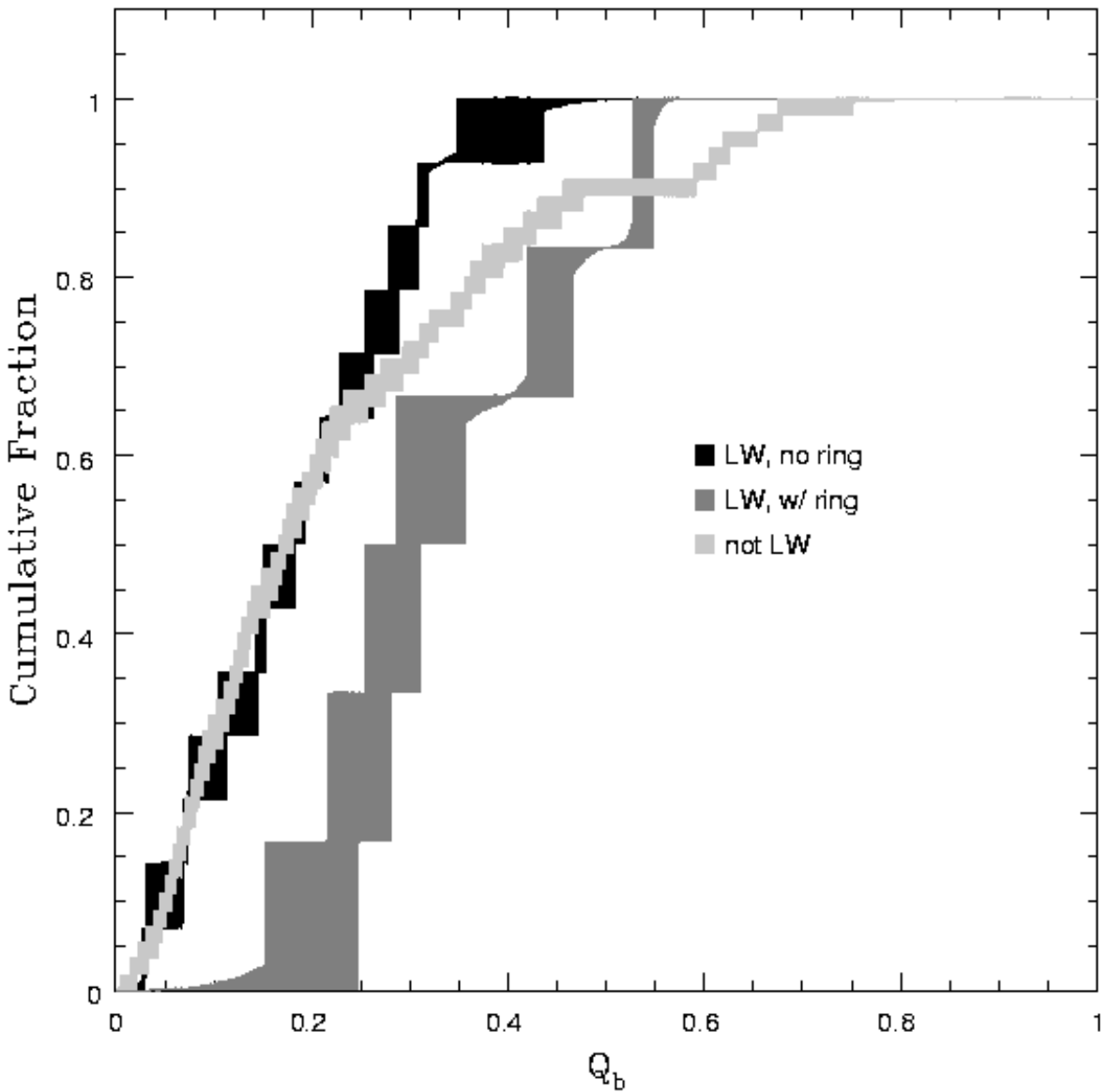


Fig. 9.— Comparison of Q_b for LW galaxies with and without circumnuclear rings. The vertical widths correspond to the central 68-percentile spread of the cumulative fraction and are due to the uncertainty in Q_b . Galaxies with circumnuclear rings are found to be more strongly barred than typical galaxies, with 1.5% probability of being drawn from the same parent population.

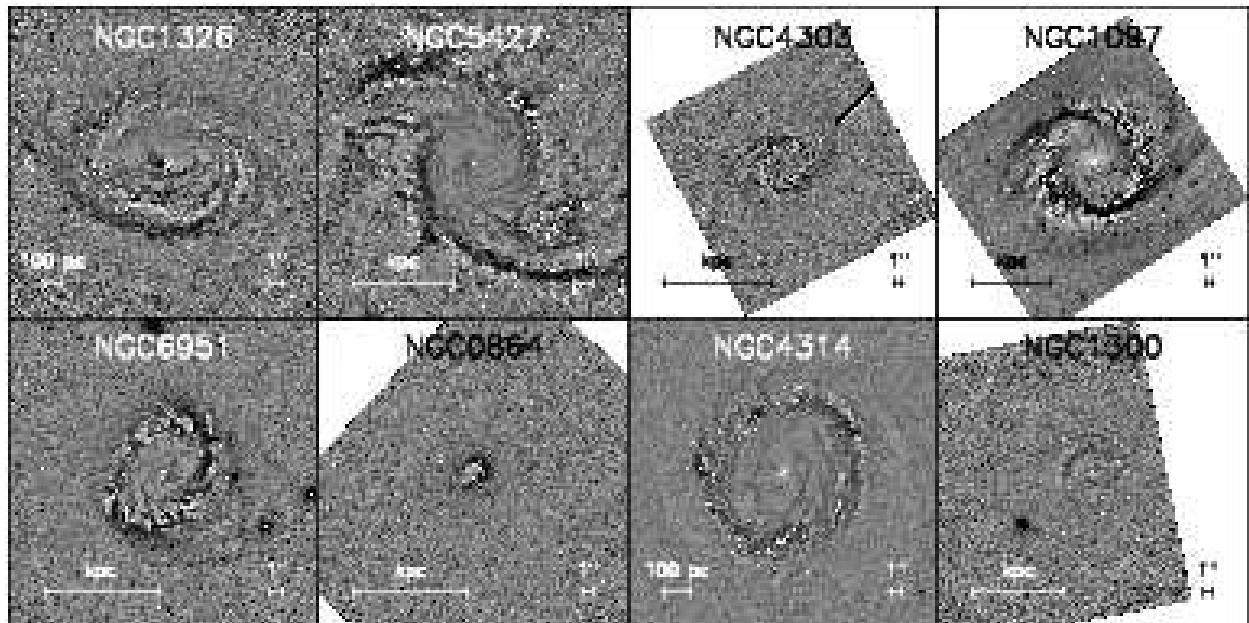


Fig. 10.— Structure maps of the eight galaxies in our sample with circumnuclear rings in order of increasing Q_b . All eight have LGD structure. Width and height are given by $0.1D_{25}$.

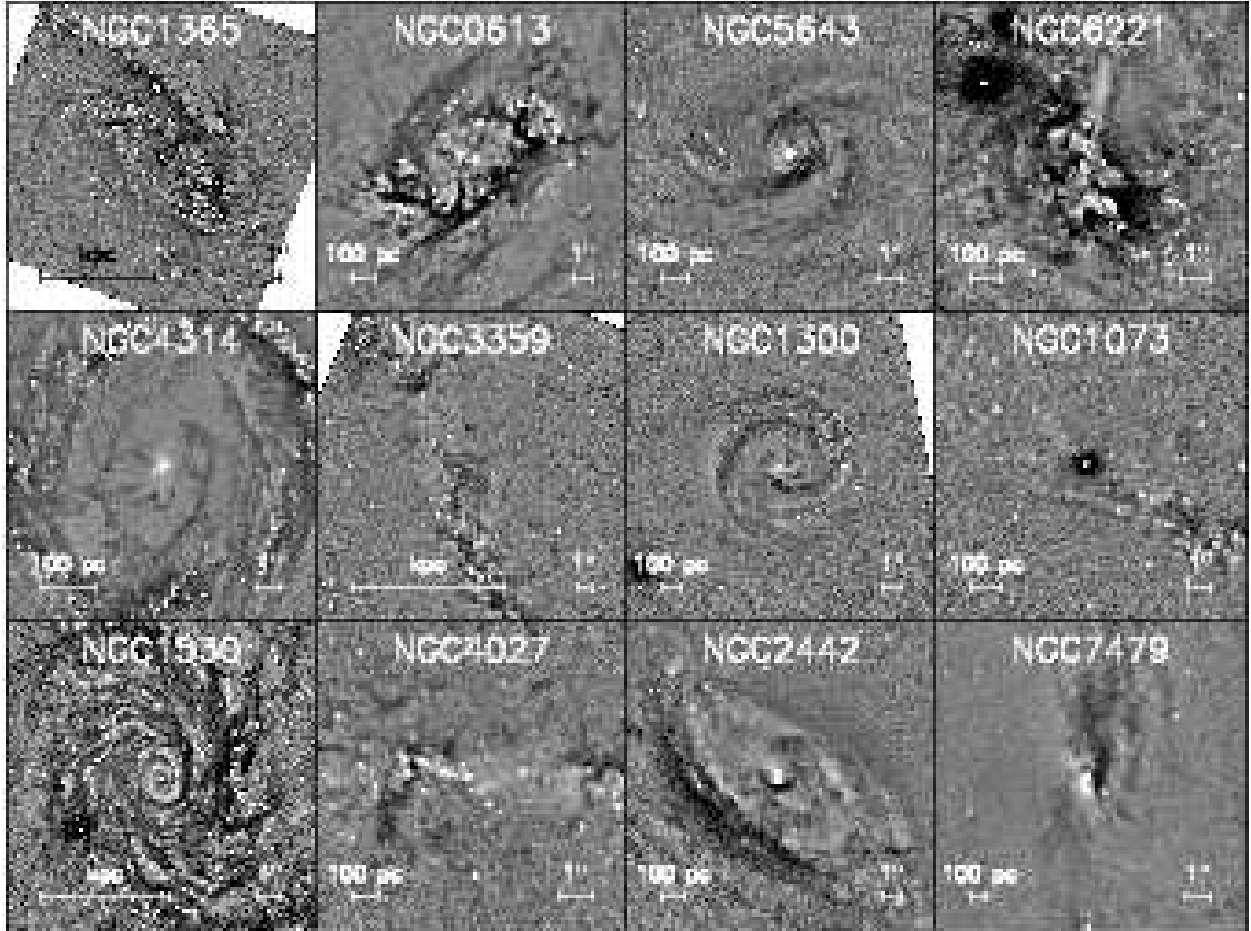


Fig. 11.— Structure maps for the 12 most strongly barred galaxies in our sample ($Q_b \geq 0.4$). Q_b increases to the right and then down. These galaxies have LGD structure (NGC1300, NGC1365, NGC5643, NGC4314, and NGC1530), chaotic nuclear structure (NGC6221, NGC3359, NGC1073, NGC4027, and NGC7479), or a chaotic nuclear spiral (NGC0613 and NGC2442). Two of the LGD spirals are associated with a circumnuclear ring (NGC1300 and NGC4314). Dark regions are due to dust; bright regions are due to emission.

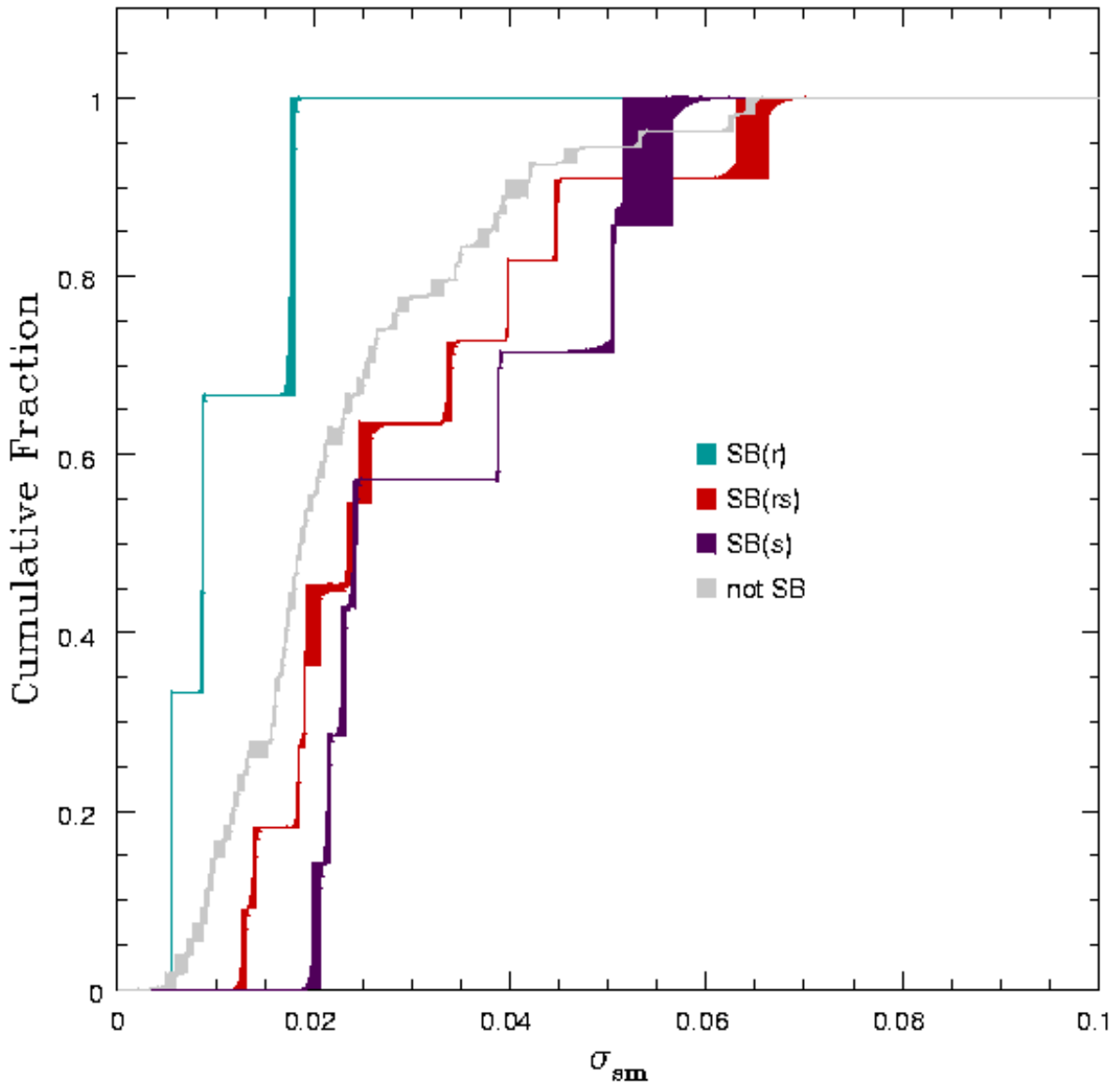


Fig. 12.— Comparisons of structure map rms σ_{sm} of SB galaxies. The vertical spreads correspond to the central 68-percentile spread of the cumulative fraction and are due to the uncertainty in Q_b . SB(r) galaxies have less dust structure than SB(rs) galaxies, which, in turn, have less dust than SB(s) galaxies. Specifically, with $\geq 99\%$ confidence, SB(r) galaxies have less central dust structure than SB(s) galaxies.